Cancer Cell
Article

Control of Tumor Bioenergetics and Survival Stress Signaling by Mitochondrial HSP90s

Young Chan Chae,[1] M. Cecilia Caino,[1] Sofia Lisanti,[1] Jagadish C. Ghosh,[1] Takehiko Dohi,[1] Nika N. Danial,[3] Jessie Villanueva,[2] Stefano Ferrero,[4] Valentina Vaira,[1,7] Luigi Santambrogio,[6] Silvano Bosari,[5] Lucia R. Languino,[1,8] Meenhard Herlyn,[2] and Dario C. Altieri[1,*]

[1]Prostate Cancer Discovery and Development Program
[2]Melanoma Research Center
The Wistar Institute, 3601 Spruce Street, Philadelphia, PA 19104, USA
[3]Dana-Farber Cancer Institute, Department of Cell Biology, Harvard Medical School, Boston, MA 02115, USA
[4]Department of Biomedical, Surgical and Dental Sciences, University of Milan Medical School and Division of Pathology
[5]Department of Clinical/Surgical Pathophysiology and Organ Transplant, University of Milan Medical School and Division of Pathology
[6]Department of Clinical/Surgical Pathophysiology and Organ Transplant, University of Milan Medical School and Division of Thoracic Surgery and Lung Transplantation
Fondazione IRCCS Cà Granda, Ospedale Maggiore Policlinico, Milan 20122, Italy
[7]Division of Pathology, Fondazione IRCCS Cà Granda, Ospedale Maggiore Policlinico, Milan 20135, Italy
[8]Department of Cancer Biology, Kimmel Cancer Center, Thomas Jefferson University, Philadelphia, PA 19107, USA
*Correspondence: daltieri@wistar.org
http://dx.doi.org/10.1016/j.ccr.2012.07.015

SUMMARY

Tumors successfully adapt to constantly changing intra- and extracellular environments, but the wirings of this process are still largely elusive. Here, we show that heat-shock-protein-90-directed protein folding in mitochondria, but not cytosol, maintains energy production in tumor cells. Interference with this process activates a signaling network that involves phosphorylation of nutrient-sensing AMP-activated kinase, inhibition of rapamycin-sensitive mTOR complex 1, induction of autophagy, and expression of an endoplasmic reticulum unfolded protein response. This signaling network confers a survival and proliferative advantage to genetically disparate tumors, and correlates with worse outcome in lung cancer patients. Therefore, mitochondrial heat shock protein 90s are adaptive regulators of tumor bioenergetics and tractable targets for cancer therapy.

INTRODUCTION

Heat shock protein-90 (HSP90) chaperones oversee protein-folding quality control in virtually every organism (Mayer, 2010). This process is essential for cellular homeostasis, buffering proteotoxic stress, and enabling cells to continuously adapt to changes in their internal and external milieus (Taipale et al., 2010). HSP90 plasticity has been traditionally linked to the diversity of its ''client proteins'', molecules that are implicated in multiple facets of cellular maintenance and require the chaperone ATPase activity for proper folding, maturation, and subcellular trafficking (Taipale et al., 2010). Successful cellular adaptation must also encompass fine-tuning of bioenergetics, nutrient sensing, and stress-response signaling, including autophagy (Yang et al., 2011), although a role of HSP90 in these pathways remains poorly defined. This may be important in cancer, where HSP90 chaperoning is universally exploited (Trepel et al., 2010), and it may help transformed cells thrive in unfavorable environments that are chronically depleted of oxygen and nutrients (Rodina et al., 2007).

Significance

Flexible adaptation to evolving environmental cues is a universal trait of human tumors, regardless of tissue of origin or genetic makeup, and it plays an important role in disease outcome. Generally considered a part of the cellular stress response, adaptive mechanisms influence cell metabolism, preserve proliferation, and promote cell survival. However, whether these pathways operate as an integrated signaling network that contributes to tumor maintenance has not been clearly delineated. The data presented here identify control of protein folding by mitochondrial, but not cytosolic, HSP90s as a global integrator of tumor bioenergetics, autophagy, and interorganelle stress-response signaling. Exploited to promote cell survival and cell proliferation in genetically disparate tumors, this adaptive network offers prime opportunities for cancer therapy.

Adding complexity to chaperone-directed protein homeostasis, or proteostasis, is the role of HSP90-like molecules compartmentalized in the endoplasmic reticulum (ER) (Richter et al., 2007) and mitochondria (Leskovar et al., 2008). The function of these specialized HSP90s in buffering the organelle protein-folding environment is beginning to emerge (Haynes and Ron, 2010), and deregulation of these pathways may contribute to human disease, including neurodegeneration (Gandhi et al., 2009) and cancer (Rodina et al., 2007). Specifically, HSP90 and its related chaperone, tumor necrosis factor receptor-associated protein-1 (TRAP-1), are abundantly present in mitochondria of tumor (though not most normal) cells (Kang et al., 2007), where they maintain organelle proteostasis (Siegelin et al., 2011) and antagonize mitochondrial permeability transition (Kang et al., 2007) mediated by the matrix immunophilin, cyclophilin D (CypD) (Green and Kroemer, 2004).

In this study, we asked whether HSP90-directed protein folding influences cellular energy production (Taipale et al., 2010), especially in tumors.

RESULTS

Regulation of Tumor Bioenergetics by Mitochondrial HSP90s

To begin exploring a role of mitochondrial chaperones in cellular energy production, we used Gamitrinib, a small-molecule inhibitor of HSP90 and TRAP-1 ATPase activity engineered to selectively accumulate in mitochondria (Kang et al., 2009). For these studies, we used 5 hr incubations with Gamitrinib, which neither reduce the viability of several independent tumor-cell types (Figure S1A available online) nor affect mitochondrial membrane potential (Figure S1B) but do create nonlethal proteotoxic stress in mitochondria, characterized by accumulation of misfolded and insoluble proteins (Siegelin et al., 2011).

Under these conditions, Gamitrinib inhibited ATP production in multiple tumor cell types in a dose-dependent manner (Figure 1A). Conversely, 17-allylamino demethoxygeldanamycin (17-AAG), which inhibits HSP90 ATPase activity in the cytosol (Trepel et al., 2010) but not in mitochondria (Kang et al., 2009), had no effect (Figure 1B). The effect of Gamitrinib on bioenergetics was selective for tumor cells, as FF2508 or MRC5 normal primary human fibroblasts were not affected (Figure 1C). Instead, Gamitrinib reduced glucose utilization (Figure 1D), extracellular lactate levels (Figure 1E), and oxygen consumption (Figure 1F), the latter a marker of impaired oxidative phosphorylation, in tumor cells. Supplementation of exogenous sodium pyruvate failed to rescue ATP production in Gamitrinib-treated tumor cells (Figure 1G). In addition, this response did not involve reactive oxygen species (ROS), which were unaffected by different concentrations of Gamitrinib (Figure 1H) for various time intervals (Figure 1I).

Small interfering RNA (siRNA) knockdown of TRAP-1 (Figure 1J), one of the HSP90 targets of Gamitrinib in mitochondria (Kang et al., 2009), similarly reduced ATP and lactate production in tumor cells (Figure 1J). A nontargeting siRNA had no effect (Figure 1J).

HSP90 Controls CypD Protein Folding and Hexokinase-II Recruitment to Tumor Mitochondria

We next asked how mitochondrial HSP90s controlled tumor bioenergetics. Mitochondrial proteotoxic stress induced by Gamitrinib (Siegelin et al., 2011) triggered concentration-dependent release of hexokinase-II (HK-II) from mitochondria, with concomitant accumulation in the cytosol (Figure 2A) HK-I expression and subcellular localization were not affected (Figure 2A). HK-II tethering to mitochondria is required for glycolysis (Vander Heiden et al., 2009) and for coupling glucose metabolism to oxidative phosphorylation. Consistent with this model, Gamitrinib-treated tumor cells exhibited decreased hexokinase activity, whereas 17-AAG had no effect (Figure 2B). siRNA knockdown of TRAP-1 gave similar results, with detachment of HK-II from tumor mitochondria (Figure 2C) and loss of hexokinase activity (Figure 2D).

In mitochondria, HSP90 binds the matrix peptidyl prolyl isomerase (PPIase), CypD (Kang et al., 2007), a component of the permeability transition pore (Green and Kroemer, 2004), which has been implicated in HK-II recruitment to the organelle outer membrane (Machida et al., 2006). Accordingly, siRNA knockdown of CypD released HK-II from mitochondria (Figure 2C) and induced loss of hexokinase activity in tumor cells (Figure 2D). Mitochondria isolated from CypD$^{-/-}$ mouse embryonic fibroblasts (MEFs) showed reduced content of HK-II compared to WT (CypD$^{+/+}$) MEFs (Figure 2E). However, transfection of these cells with a WT CypD cDNA restored binding of HK-II to mitochondria, whereas an H168Q CypD mutant defective in PPIase activity, or empty vector, had no effect (Figure 2F). As a control, the expression of voltage-dependent anion channel (VDAC) was not affected (Figure 2F). We next asked whether CypD retention of HK-II involved chaperone-directed protein folding. Inhibition of mitochondrial HSP90s by Gamitrinib rendered CypD insoluble at increasing detergent concentrations, which suggests protein misfolding and aggregation, compared to untreated cultures (Figure 2G). In contrast, the folding of another mitochondrial protein, COX-IV was indistinguishable in control or Gamitrinib-treated cells, and VDAC remained insoluble at all detergent concentrations used (Figure 2G).

Regulation of Energy-Sensing Pathways by Mitochondrial HSP90s

The downstream implications of defective HK-II-dependent bioenergetics were next investigated. First, siRNA silencing of the energy-sensing AMP-activated kinase (AMPK) (Mihaylova and Shaw, 2011) did not affect HK-II association with tumor mitochondria (Figure 3A) positioning its function downstream of HK-II-directed bioenergetics (Mihaylova and Shaw, 2011). Conversely, tumor cells treated with Gamitrinib, but not 17-AAG, exhibited concentration-dependent phosphorylation of AMPK (Figure 3B; Figure S2A). This response occurred within 30 min of Gamitrinib treatment, remained sustained for 9 hr (Figure 3C), and was quantitatively more robust than that induced by metformin, a known AMPK inducer (Figure 3D). Total AMPK levels were unaffected (Figures 3B–3D), and the combination of metformin plus Gamitrinib did not further stimulate AMPK phosphorylation (Figure 3D).

Silencing of AMPK (Figure S2B) or its main upstream activator, the serine/threonine kinase LKB1 (Mihaylova and Shaw, 2011) (Figure S2C), using multiple independent siRNA sequences suppressed AMPK phosphorylation mediated by Gamitrinib (Figures S2B and S2C). This response was selective for tumor cells, as FF2508 or MRC5 primary human fibroblasts did not activate AMPK in response to Gamitrinib, consistent with the absence

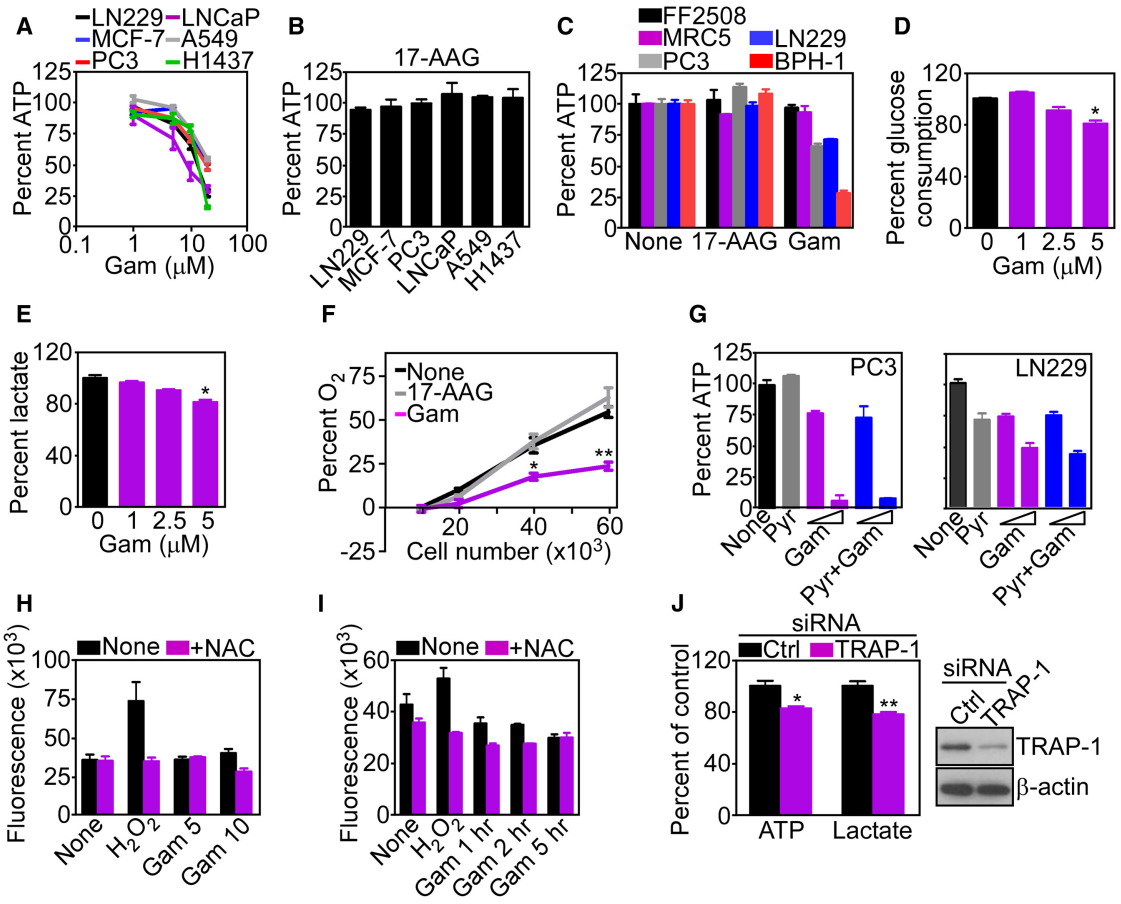

Figure 1. Mitochondrial HSP90 Regulation of Tumor Bioenergetics

(A) Breast (MCF-7), prostate (PC3, LNCaP), lung (A549, H1473), and brain (glioblastoma, LN229) tumor cell lines were treated with the indicated concentrations of Gamitrinib (Gam) for 5 hr and analyzed for ATP production. Mean ± SEM (n = 3).

(B) The indicated tumor cell lines were treated with 17-AAG (20 μM) for 5 hr and analyzed for ATP production. Mean ± SEM (n = 3).

(C) The indicated normal (FF2508, MRC5) or tumor (LN229, PC3, BPH-1) cell lines were incubated with 17-AAG or Gamitrinib (10 μM) for 5 hr and analyzed for ATP production. Mean ± SEM (n = 3).

(D and E) LN229 cells were treated with the indicated concentrations of Gamitrinib for 5 hr and analyzed for glucose consumption (D) or extracellular lactate content (E). Mean ± SEM (n = 3); *p = 0.015-0.022.

(F) LN229 cells were plated at the indicated number, treated with vehicle, Gamitrinib, or 17-AAG (5 μM), and analyzed for O_2 consumption by a fluorimetric assay. Mean ± SEM (n = 3), *p = 0.019; **p = 0.001.

(G) PC3 or LN229 cells were incubated with sodium pyruvate (Pyr, 1 mM) in the presence (5 or 10 μM, respectively) or absence (None) of Gamitrinib for 7 hr and analyzed for ATP production. Mean ± SD of replicates (n = 2).

(H) LN229 cells were labeled with the fluorescent dye H_2-DCFA (6 μM), treated with Gamitrinib (5–10 μM), and analyzed for changes in fluorescence expression in a luminometer, with or without the antioxidant *N*-acetyl-L-cysteine (10 mM, NAC). H_2O_2 (5 mM) was used as control. Mean ± SEM (n = 4).

(I) H_2-DCFA-labeled LN229 cells were treated with 10 μM Gamitrinib for the indicated time intervals and analyzed for changes in ROS production at the indicated time intervals with or without NAC. H_2O_2 was a control. Mean ± SEM (n = 3).

(J) LN229 transfected with control (Ctrl) or TRAP-1-directed siRNA were analyzed for changes in ATP production or extracellular lactate content (left) or TRAP-1 protein level (right). Mean ± SEM (n = 3); *p = 0.017; **p = 0.005.

See also Figure S1.

of TRAP-1 in normal mitochondria (Figure S2D) (Kang et al., 2007). In complementary studies, TRAP-1 knockdown in tumor cells using various siRNA sequences (Figure 3E) stimulated AMPK phosphorylation and induced detachment of HK-II, but not VDAC or COX-IV, from mitochondria (Figure 3E).

Downstream of AMPK activation, Gamitrinib treatment inhibited the rapamycin-sensitive mammalian target of rapamycin complex-1 (mTORC1) in tumor cells (Wullschleger et al., 2006), with loss of phosphorylation of mTOR and its downstream targets, p70S6 and 4EBP1 (Figures 3F and 3G). In these experiments, 17-AAG had no effect (Figure 3G), and total mTORC1 protein content was unchanged (Figures 3F and 3G). Consistent with a selectivity of this pathway for tumor cells, Gamitrinib treatment of nontransformed NIH 3T3 fibroblasts did not affect ATP production (Figure S2E), or AMPK or mTORC1 phosphorylation (Figure 3G). siRNA silencing of LKB1 (Figure S2F) or AMPK (Figure S2G) partially restored phosphorylation of mTOR, p70S6, and 4EBP1 in Gamitrinib-treated tumor cells (Figures S2F and

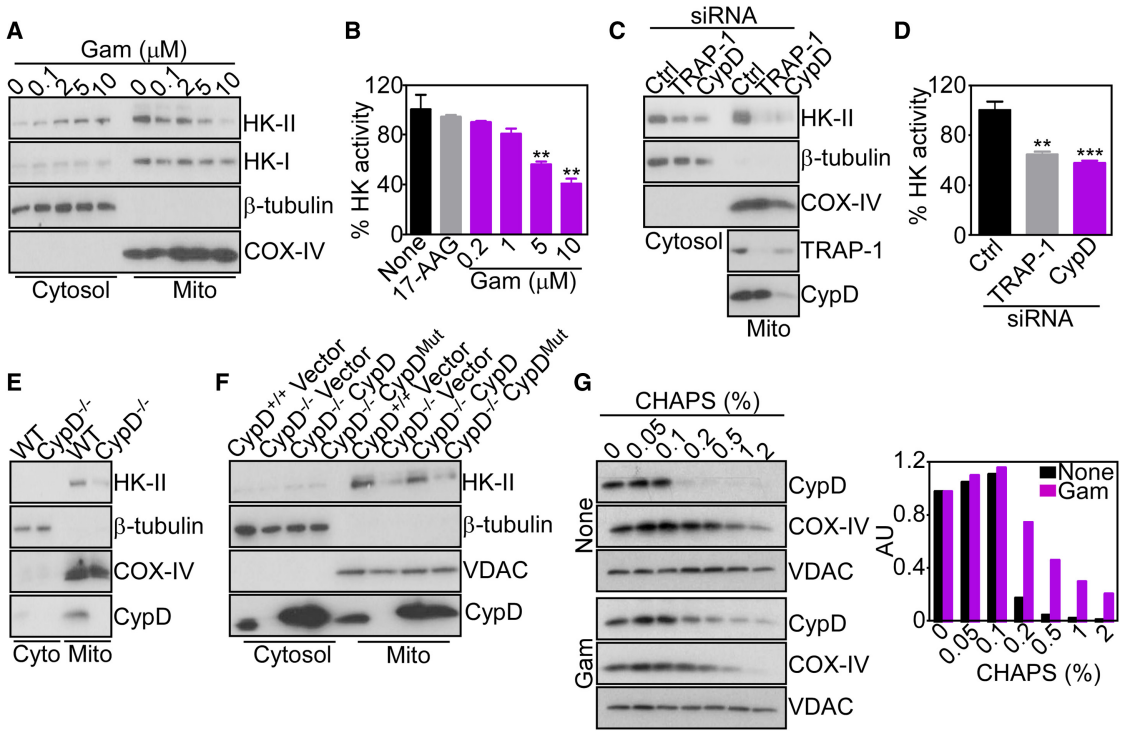

Figure 2. Mitochondrial HSP90 Control of CypD Folding and HK-II Recruitment

(A) LN229 cells were treated with Gamitrinib (Gam), and cytosolic or mitochondrial (Mito) fractions were analyzed after 5 hr by western blotting. COX-IV was a mitochondrial marker.

(B) LN229 cells were treated with 17-AAG (10 μM) or Gamitrinib (0.2–10 μM), and mitochondrial fractions were analyzed for hexokinase activity after 5 hr. Mean ± SD (n = 2); **p = 0.005–0.004.

(C) LN229 cells were transfected with control (Ctrl) or with CypD- or TRAP-1-directed siRNA, and isolated mitochondrial (Mito) or cytosol fractions were analyzed by western blotting after 48 hr.

(D) Mitochondrial fractions from LN229 cells transfected as in (C) were analyzed for hexokinase activity after 48 hr. Mean ± SD (n = 2); ***p = 0.0009; **p = 0.0024.

(E) Mitochondrial (Mito) or cytosol (Cyto) fractions from WT ($CypD^{+/+}$) or $CypD^{-/-}$ MEFs were analyzed by western blotting.

(F) $CypD^{+/+}$, $CypD^{-/-}$, or $CypD^{-/-}$ MEFs reconstituted with WT or PPIase-defective H168Q mutant CypD cDNA were fractionated in cytosol or mitochondrial (Mito) extracts, and analyzed by western blotting.

(G) LN229 cells were left untreated (None) or incubated with Gamitrinib (5 μM) and mixed with the indicated increasing concentrations of CHAPS. Detergent-insoluble proteins were analyzed by western blotting. The bar graph shows densitometric quantification of protein bands. AU, arbitrary units.

S2G). Conversely, knockdown of HK-II enhanced the effect of Gamitrinib, with increased AMPK phosphorylation and mTORC1 inhibition (Figure S2H).

Further supporting a role of defective bioenergetics in this response, exposure of tumor cells to the nonhydrolyzable glucose analog, 2-deoxy glucose (2-DG), which mimics energy starvation (Egan et al., 2011), reproduced the effect of Gamitrinib, with strong activation of AMPK and suppression of mTOR, p70S6, and 4EBP1 phosphorylation (Figure 3H).

Mitochondrial Proteotoxic Stress Activates Prosurvival Autophagy

The implication of mTORC1 inhibition by mitochondrial proteotoxic stress was next investigated. Consistent with an inhibitory role of mTORC1 on autophagy, and in agreement with recent observations (Siegelin et al., 2011), Gamitrinib strongly induced autophagy in tumor cells, with conversion of microtubule-associated protein light-chain-3 (LC3-II) to a lipidated form (Figure 4A) and appearance of a punctate fluorescence pattern of LC3-CFP staining in transfected cells (Figures S3A and S3B). This induction of autophagy required AMPK, as siRNA silencing of LKB1 (Figure 4B) or AMPK (Figure 4C) suppressed LC3-II conversion (Figures 4B and 4C) and autophagosome formation (Figures S3A and S3B) induced by Gamitrinib. As control, siRNA silencing of the essential autophagy gene, ATG5, produced similar results (Figure 4D; Figures S3A and S3B), consistent with recent observations (Siegelin et al., 2011).

We next asked whether autophagy activated by mitochondrial proteotoxic stress influenced tumor cell viability (Siegelin et al., 2011). Inhibition of phagosome formation by 3-methyadenine (3-MA) (Figure 4E), or siRNA knockdown of ATG5 (Figure 4F) (Siegelin et al., 2011) or LKB1 (Figure 4G), enhanced tumor cell killing mediated by suboptimal concentrations of Gamitrinib. Similarly, siRNA silencing of HK-II (Figure S3D) potentiated Gamitrinib-induced tumor cell death (Figure 4H), as characterized by increased Annexin V labeling, compared to control transfectants (Figure 4I). In contrast, the combination of 17-AAG plus 3-MA (Figure 4E), or 17-AAG plus siRNA silencing of LKB1 (Figure 4G) or HK-II (Figure 4H), did not decrease tumor cell viability compared to each treatment alone.

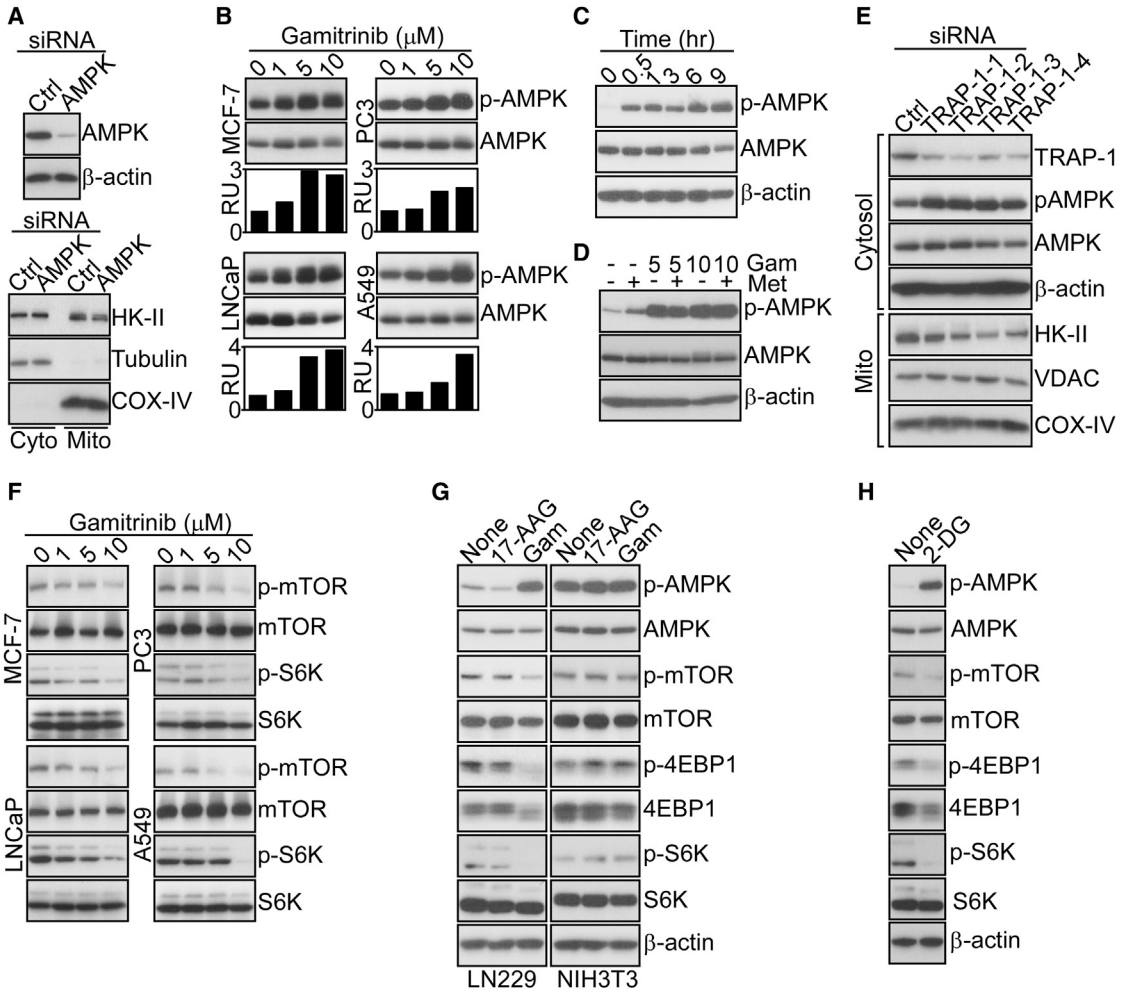

Figure 3. Modulation of AMPK and mTORC1 Signaling by Mitochondrial HSP90s

(A) LN229 cells were transfected with control (Ctrl) or AMPK-directed siRNA, and total cell extracts (top) or isolated cytosol (Cyto) or mitochondrial (Mito) fractions (bottom) were analyzed by western blotting.

(B) The various tumor cell lines were treated with the indicated concentrations of Gamitrinib, and analyzed by western blotting after 5 hr. The bar graphs show densitometric quantification of protein bands. RU, relative units.

(C) Gamitrinib-treated (10 μM) LN229 cells were analyzed at the indicated time intervals by western blotting.

(D) LN229 cells were treated with metformin (Met, 5 mM) in the presence or absence of Gamitrinib (Gam, 5–10 μM) and analyzed after 12 hr by western blotting.

(E) LN229 cells were transfected with control (Ctrl) or the indicated individual siRNA sequences against TRAP-1, and isolated cytosol or mitochondrial (Mito) fractions were analyzed by western blotting.

(F) The indicated tumor cell types were treated with increasing concentrations of Gamitrinib and analyzed after 12 hr by western blotting.

(G) Tumor (LN229) or normal (NIH 3T3) cell types were treated with Gamitrinib or 17-AAG (10 μM) and analyzed after 12 hr by western blotting.

(H) LN229 cells were treated with 2-DG (25 mM) and analyzed after 12 hr by western blotting.

See also Figure S2.

Metabolic Interorganelle ER Signaling by Mitochondrial HSP90s

Defective mitochondrial bioenergetics impair protein posttranslational modifications in the ER (Kaufman et al., 2002), which may trigger an unfolded protein response (UPR) (Hetz and Glimcher, 2009). Consistent with this model, tumor cells treated with Gamitrinib exhibited increased expression of inositol-requiring-1 (IRE-1) kinase (Figure 5A), an ER stress sensor (Hetz and Glimcher, 2009), and de novo mRNA splicing, i.e., activation, of its target, X-box protein-1 (XBP1) (Figure 5B). This was associated with activation of other ER UPR branches (Hetz and Glimcher, 2009), with activating transcription factor-6 (ATF-6)-mediated upregulation of the ER chaperone GRP78 (Figure 5C; Figure S4A), and PKR-like endoplasmic reticulum kinase (PERK) induction of transcription factors CCAAT-enhancer binding protein (C/EBPβ) and C/EBP homology protein (CHOP) (Figure 5C; Figures S4B and S4C) (Siegelin et al., 2011). Gamitrinib also induced transient phosphorylation of PERK-regulated eIF2α in tumor cells (Figure 5C). Upregulation of ER stress markers by Gamitrinib occurred within 1 hr of treatment (Figure S4A), and over a broad range of concentrations (Figure S4B), similar to the response induced by the ER stressor tunicamycin (Figure S4D).

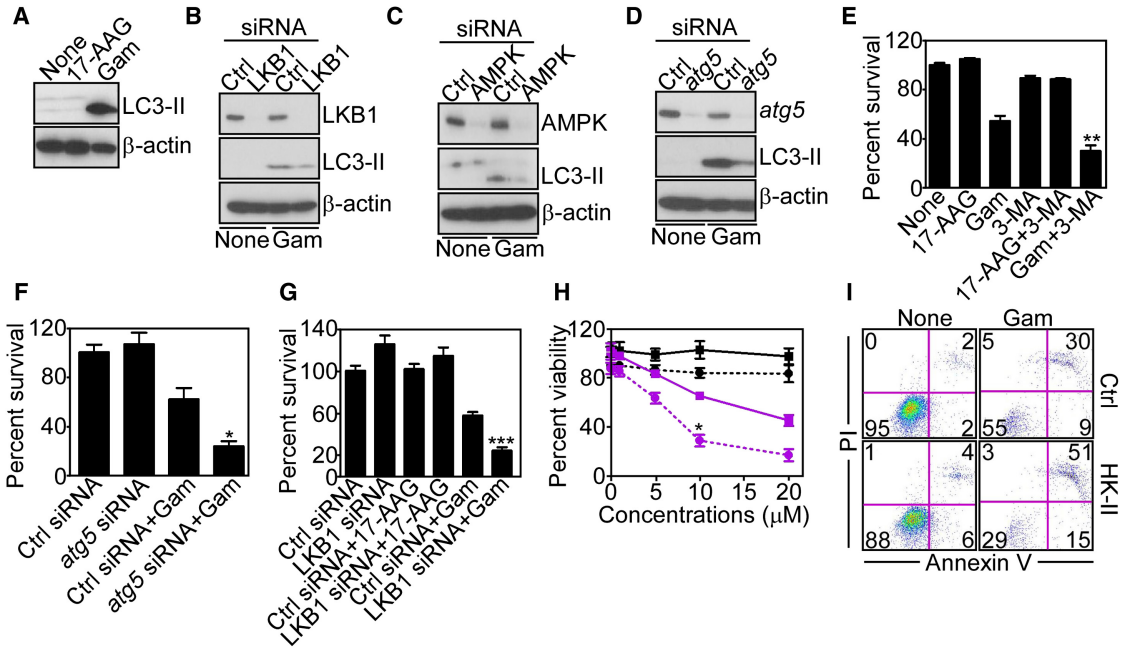

Figure 4. Mitochondrial Proteotoxic Stress Stimulates Autophagy

(A) LN229 cells treated with Gamitrinib or 17-AAG (10 μM) for 12 hr were analyzed by western blotting.

(B–D) LN229 cells were transfected with control (Ctrl), or with LKB1-, AMPK-, or ATG5-directed (B–D, respectively) siRNA, treated with vehicle or Gamitrinib (10 μM), and analyzed after 48 hr by western blotting.

(E) LN229 cells were treated with the inhibitor of phagosome formation, 3-MA, treated with Gamitrinib or 17-AAG (10 μM), and analyzed for cell viability by 3-(4,5-dimethylthiazol-2-YI)-2,5-diphenyltetrazolium bromide (MTT). Mean ± SD (n = 2); **p = 0.0072.

(F and G) LN229 cells were transfected with control siRNA (Ctrl) or with ATG5- or LKB1-directed siRNA (F and G, respectively), incubated with 17-AAG or Gamitrinib (10 μM) (G), and analyzed for cell viability by MTT. Mean ± SEM (n = 4). *p = 0.02; ***p < 0.0004.

(H) LN229 cells were transfected with control (squares) or HK-II-directed (circles) siRNA, treated with increasing concentrations of 17-AAG (black) or Gamitrinib (purple), and analyzed after 12 hr for cell viability by MTT. Mean ± SD (n = 2); *p = 0.02.

(I) LN229 cells were transfected with control (Ctrl) or HK-II-directed siRNA, treated with vehicle (None) or Gamitrinib, and analyzed for Annexin V and propidium iodide staining by multiparametric flow cytometry. The percentage of cells in each quadrant is indicated.

See also Figure S3.

Next, we asked whether this ER UPR involved de novo gene expression. Gamitrinib treatment resulted in time-dependent upregulation of CHOP, C/EBPβ, and GRP78 mRNA levels (Figure 5D). Similarly, exposure of tumor cells to Gamitrinib, 2-DG, or tunicamycin all resulted in transcriptional activation of IRE-1, ATF6, and PERK response elements in luciferase promoter analysis (Figures 5E and 5F). A minimal CHOP promoter region was also transcriptionally induced by Gamitrinib (Figure 5F).

A mechanistic link between Gamitrinib-induced ER UPR and defective mitochondrial bioenergetics was next investigated. First, exposure of tumor cells to the mitochondrial uncoupler carbonyl cyanide 3-chlorophenylhydrazone (CCCP) reproduced the effect of Gamitrinib, with time-dependent phosphorylation of AMPK (Figure S4E), upregulation of CHOP, C/EBPβ, and GRP78, inhibition of 4EBP1 phosphorylation, and stimulation of LC3-II conversion (Figure 5G). In contrast, incubation of tumor cells with inhibitory concentrations of the ROS scavenger *N*-acetyl-L-cysteine (NAC) did not affect Gamitrinib-induced phosphorylation of AMPK or its target acetyl-CoA carboxylase (ACC), or upregulation of ER stress markers (Figure 5H). Conversely, energy deprivation, or impaired N-linked glycosylation (Kurtoglu et al., 2007), caused by 2-DG mimicked the effect of Gamitrinib and resulted in concentration (Figure S4F)- and time (Figure S4G)-dependent upregulation of ER UPR in tumor cells. When combined with 2-DG, Gamitrinib maximally stimulated AMPK and eIF2α phosphorylation in tumor cells (Figure S4H). This resulted in complete translational repression, and ablation of GRP78, CHOP, or C/EBPβ levels (Figure S4H). Functionally, this was associated with enhanced tumor cell killing by suboptimal concentrations of Gamitrinib, compared to each agent alone (Figure S4I).

In parallel experiments, exposure of tumor cells to low-glucose-containing medium (5 mM) stimulated AMPK phosphorylation and increased the expression of CHOP, C/EBPβ, and GRP78 (Figure 5I). Supplementation of tumor cells with high-glucose-containing medium partially reversed this response and attenuated the expression of ER UPR markers and AMPK phosphorylation in the presence of Gamitrinib (Figure 5I). Similar to ATP production (Figure 1G), addition of exogenous sodium pyruvate did not modulate AMPK or ER UPR signaling by Gamitrinib (Figure 5J).

Cytoprotective Role of ER UPR Induced by Gamitrinib

We next mapped the requirements of Gamitrinib-induced ER UPR. First, siRNA knockdown of HK-II was insufficient, alone, to upregulate the expression of CHOP or GRP78, promote

AMPK phosphorylation, or stimulate LC3-II conversion in tumor cells (Figure 6A). However, the combination of HK-II knockdown plus Gamitrinib enhanced AMPK phosphorylation, ER UPR induction, and autophagy in tumor cells (Figure 6A). This pathway still depended on impaired tumor bioenergetics, as siRNA knockdown of AMPK (Figure 6B) or LKB1 (Figure 6C) attenuated Gamitrinib-induced phosphorylation of AMPK, ACC, and the upregulation of ER UPR markers (Figures 6B and 6C). Conversely, siRNA silencing of the ER UPR effector GRP78 (Figure 6D; Figure S5) did not affect phosphorylation of AMPK or mTORC1 kinases in the presence of Gamitrinib, positioning GRP78 induction downstream of impaired ATP production (Figure 1). Reciprocally, siRNA knockdown of the ER stress sensor IRE-1 did not significantly affect the induction of UPR markers by Gamitrinib (Figure 6E). In contrast, knockdown of PERK, alone or in combination with IRE-1 silencing, inhibited the expression of CHOP and C/EBPβ and abolished eIF2α phosphorylation induced by Gamitrinib, whereas GRP78 was not significantly affected, and no changes were observed in LC3 conversion (Figure 6E). In all silencing experiments, a nontargeting siRNA was ineffective (Figures 6A–6E).

Next, we asked whether components of this ER UPR influenced tumor cell functions. Silencing of GRP78 using multiple independent siRNA sequences inhibited tumor cell proliferation compared to control siRNA transfectants (Figure 6F). Similar results were obtained in different cell types (Figure 6G), indicating a general requirement of GRP78 for tumor cell proliferation. In addition, GRP78 knockdown decreased the viability of selected tumor cell types including prostate cancer PC3 or LNCaP cells (Figure 6H). In contrast, IRE-1 or PERK knockdown, alone or in combination, did not reduce tumor cell viability in the presence or absence of Gamitrinib (Figure 6I).

Chaperone-Regulated Bioenergetics Controls Tumor Maintenance

Next, we asked whether the signaling pathway controlled by mitochondrial HSP90s was important for tumor maintenance. In a first model, we looked at melanoma cells, where a V600E mutation of the BRAF oncogene results in ERK-mediated inhibitory phosphorylation of LKB1 and suppression of AMPK activation (Zheng et al., 2009). Accordingly, two BRAF mutant melanoma cell lines, which exhibited hyperphosphorylated ERK, failed to activate AMPK in response to Gamitrinib (Figure 7A; Figure S6A). Conversely, Gamitrinib induced AMPK phosphorylation in WT BRAF melanoma cells with low levels of phosphorylated ERK (Figure 7A; Figure S6A). 17-AAG had no effect on AMPK activation in WT or mutant BRAF melanoma cells (Figure 7A; Figure S6A). Similar to the data above, AMPK activation by mitochondrial stress activated autophagy in WT BRAF cells, whereas BRAF mutant cells did not increase autophagy in response to Gamitrinib (Figure 7B). Functionally, mutant BRAF melanoma cells exhibited increased sensitivity to Gamitrinib-induced cell death compared to WT BRAF melanoma cells (IC_{50} BRAF V600E, 1.95 ± 0.21; IC_{50} BRAF WT, 6 ± 1.4) (Figure 7C). This response was due to differential activation of compensatory autophagy, as siRNA knockdown of AMPK suppressed autophagy in WT BRAF cells (Figure 7D; Figure S6B) and enhanced their sensitivity to Gamitrinib-mediated killing (Figure 7E; Figure S6C). As control, an inhibitor of MEK, U0126, partially restored AMPK phosphorylation in mutant BRAF melanoma cells after Gamitrinib treatment (Figure S6D). To examine this pathway in a more disease-relevant model, we next reconstituted melanoma cell growth in 3-D spheroids embedded in a collagen matrix (Villanueva et al., 2010). In this system, low concentrations of Gamitrinib (1–3 μM) efficiently killed mutant BRAF melanoma cells, whereas WT BRAF spheroids were resistant to cell death (Figure 7F).

Mitochondrial HSP90-Directed Bioenergetics Influences Tumor Outcome

To determine whether mitochondrial HSP90-directed signaling occurred in vivo, we next examined a genetic model of prostate cancer in immunocompetent TRAMP (transgenic adenocarcinoma of the mouse prostate) mice treated systemically with Gamitrinib (Kang et al., 2011). In this model, Gamitrinib inhibited primary and metastatic prostate cancer growth, but did not affect prostatic intraepithelial neoplasia (PIN) (Kang et al., 2011). Here, Gamitrinib treatment was associated with increased expression of phosphorylated AMPK, induction of autophagy, i.e., LC3 conversion, and upregulation of GRP78 in PIN lesions, but not in normal prostate (Figure 8A). Prostate tissues from TRAMP mice treated with vehicle did not express these markers (Figure 8A).

We next looked at primary human tumor specimens, and we focused on a potential role of the ER stress chaperone GRP78 in disease progression in vivo. Except for lymphoma, GRP78 was strongly and uniformly upregulated in the tumor cell population of a large panel of genetically heterogeneous cancers, as shown by tissue microarray (TMA; Figure 8B; Figure S7A). Accordingly, GRP78 was abundantly expressed in non-small-cell lung cancer (NSCLC) patients (Table S1) with adenocarcinoma (AdCa) or squamous cell carcinoma (SCC) (Figures 8C and 8D), regardless of tumor stage (Figure S7B), or lymph node metastasis (Figure S7C). Conversely, GRP78 was undetectable in the normal epithelium of the lung (Figures 8C and 8D). When stratified for disease outcome, patients with lung AdCa expressing GRP78 had considerably shorter overall survival compared to those with low to undetectable GRP78 (Figure 8E).

Based on these results, we asked whether deregulated expression of GRP78 influenced cell proliferation and/or survival of lung cancer cells. siRNA silencing of GRP78 (Figure 8F) induced loss of viability of H1299 and A549 lung cancer cells, whereas H1457 and H1650 cells were only partially affected (Figure 8G). Similar to other tumor types (Figures 6F and 6G), silencing of GRP78 suppressed proliferation of all lung cancer cells tested (Figure 8H), whereas a nontargeting siRNA had no effect (Figures 8G and 8H).

DISCUSSION

In this study, we have shown that HSP90s compartmentalized in mitochondria (Kang et al., 2007) are essential regulators of bioenergetics in tumor cells but not normal cells. This pathway controls both glycolysis and oxidative phosphorylation and involves chaperone-dependent retention of HK-II (Vander Heiden et al., 2009) to the organelle outer membrane (Majewski et al., 2004). Interference with chaperone control of mitochondrial protein folding causes acute decrease in ATP production

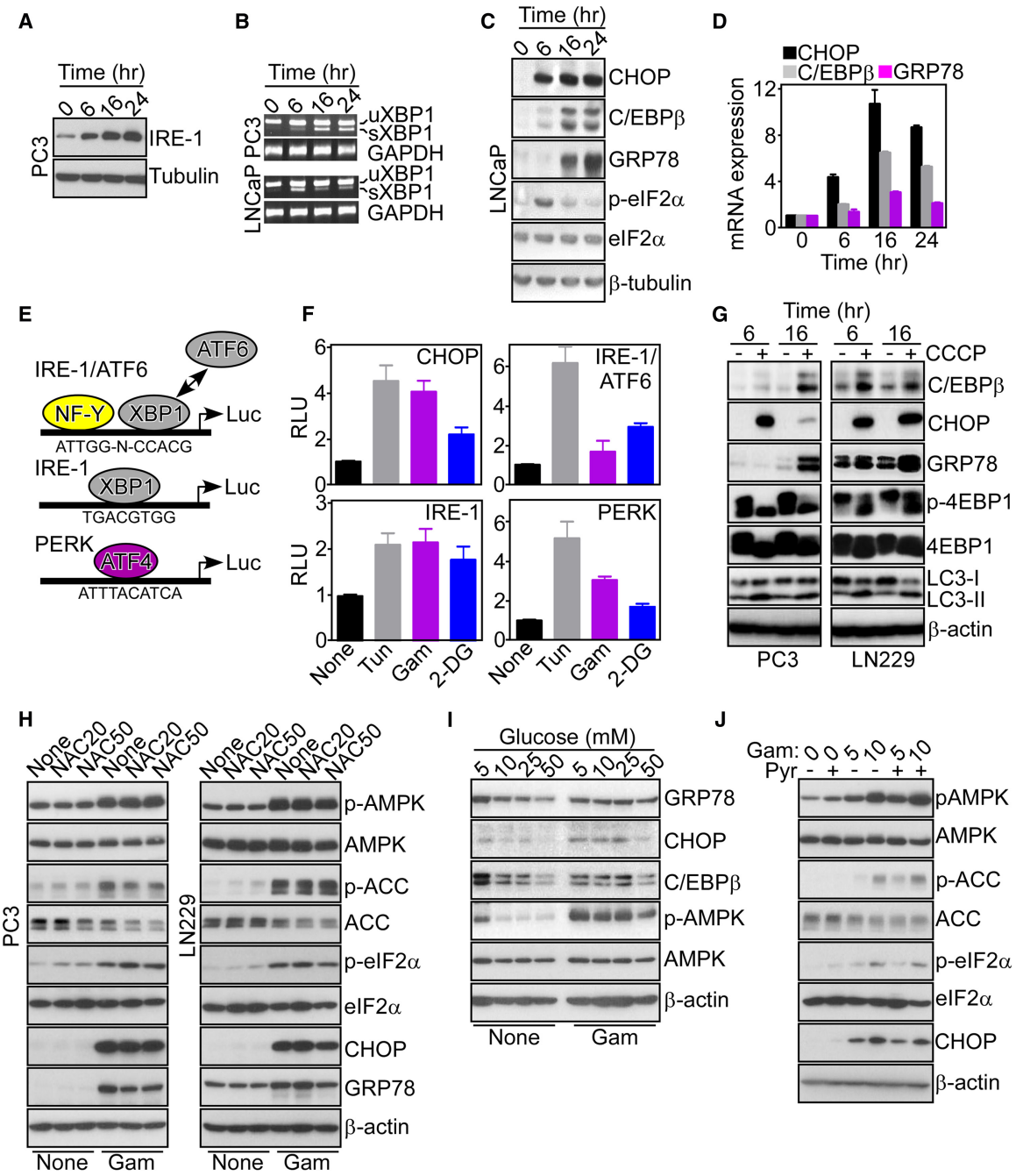

Figure 5. Regulation of ER UPR by Mitochondrial HSP90s

(A) PC3 cells were incubated with Gamitrinib (5 μM) and analyzed at the indicated time intervals by western blotting.

(B) Gamitrinib-treated tumor cells were harvested at the indicated time intervals, and total RNA was amplified with primers to detect spliced (s) or unspliced (u) XBP1 mRNA transcripts. GAPDH was used as a control.

(C) LNCaP cells were treated with Gamitrinib and analyzed at the indicated time intervals by western blotting.

(D) Gamitrinib-treated LNCaP cells were harvested at the indicated time intervals and analyzed for changes in CHOP, C/EBPβ, or GRP78 mRNA expression by quantitative PCR. Mean ± SEM of replicates of a representative experiment (n = 3).

(E) Schematic diagram of ER stress luciferase-promoter reporter constructs used in this study.

(F) PC3 cells were transfected with the indicated luciferase-promoter reporter constructs, or with a CHOP minimal promoter upstream of a luciferase gene, incubated with Gamitrinib (5 μM), tunicamycin (Tun, 2.5 μg/ml), or 2-DG (25 mM), and analyzed for changes in luciferase expression in a luminometer after 20 hr. Mean ± SEM (n = 4). None, untreated.

(G) PC3 cells were treated in the presence (+) or absence (−) of the mitochondrial uncoupler CCCP and analyzed after 6 or 16 hr by western blotting.

(H) The indicated tumor cell types were incubated without (None) or with 5 μM Gamitrinib in the presence or absence of the indicated concentrations of NAC (20 or 50 μM) and analyzed after 6 hr by western blotting.

and activation of an integrated signaling network, with phosphorylation of AMPK (Mihaylova and Shaw, 2011), inhibition of mTORC1 (Wullschleger et al., 2006), induction of autophagy (Yang et al., 2011), and stimulation of ER UPR (Hetz and Glimcher, 2009). Functionally, this pathway provides proliferative and cytoprotective compensatory signals for tumor cells, has been recapitulated in a genetic mouse model of prostate cancer in immunocompetent animals (Kang et al., 2011), and correlates with shortened overall survival in patients with lung adenocarcinoma.

CypD is the only known component of a mitochondrial permeability transition pore (Green and Kroemer, 2004) that is required for cell death triggered by certain stimuli, for instance, oxidative stress (Baines et al., 2005; Nakagawa et al., 2005). How this process is regulated is still a matter of debate, but recent evidence has pointed to chaperone-directed (re)folding of CypD as a potential mechanism to preserve mitochondrial integrity, and to antagonize apoptosis, selectively in tumor cells (Kang et al., 2007). The structural requirements of potential HSP90-CypD protein complexes in mitochondria (Kang et al., 2007) remain to be fully elucidated. However, complete suppression of chaperone ATPase activity with Gamitrinib (Kang et al., 2009) results in misfolding and aggregation of CypD (this study), culminating in acute permeability transition and CypD-dependent cell death (Kang et al., 2009). Conversely, titrating the extent of chaperone inhibition using suboptimal concentrations of Gamitrinib and shorter incubation times (Siegelin et al., 2011) uncovered additional functional roles of this pathway, and in particular a mechanism of CypD conformation-dependent retention of HK-II to the outer mitochondrial membrane. In this context, detachment of HK-II after nonlethal mitochondrial proteotoxic stress (Siegelin et al., 2011) is expected to lower an antiapoptotic threshold maintained by growth factor-Akt signaling (Robey and Hay, 2006), but, even more importantly, to impair aerobic glycolysis, the main energy source for tumor cells (Vander Heiden et al., 2009). Whether mitochondrial proteotoxic stress affects other pathways of ATP or biomass production in tumors remains to be determined. However, the inhibition of oxygen consumption observed here after Gamitrinib treatment, combined with the inability of exogenous pyruvate to restore ATP production under these conditions, suggest that organelle HSP90s may also contribute to oxidative phosphorylation. The details of this potential response are presently unknown, but it is intriguing that loss of HK-II (Vander Heiden et al., 2009) has been shown to shift tumor bioenergetics from aerobic glycolysis toward oxidative phosphorylation (Wolf et al., 2011), potentially rendering tumor cells especially sensitive to the pathway of mitochondrial proteotoxicity described here.

Consistent with current models of bioenergetics, loss of ATP production after mitochondrial proteotoxic stress resulted in downstream activation of an LKB1-AMPK signaling axis in tumor cells. These molecules participate in tumor suppression, and a growing number of cancers harbor LKB1-inactivating mutations (Hezel and Bardeesy, 2008). Here, however, activation of the LKB1-AMPK pathway was exploited for tumor cell survival via stimulation of autophagy (Mihaylova and Shaw, 2011). This may reflect release of mTORC1 inhibition on autophagy initiation (Gwinn et al., 2008; Inoki et al., 2003) and/or direct phosphorylation of the ULK-1-containing autophagy complex by AMPK (Egan et al., 2011). How common is the exploitation of LKB1-AMPK signaling for tumor cell survival in vivo remains to be determined. However, AMPK phosphorylation has been observed in hypoxic tumors deprived of nutrients (Laderoute et al., 2006). It was prominently induced in PIN lesions of TRAMP mice treated with therapeutic concentrations of Gamitrinib (Kang et al., 2011; this study). In addition, downstream activation of autophagy is being increasingly recognized as a major driver of tumor maintenance, potentially at later stages of disease progression (Yang et al., 2011). In melanoma, where AMPK can be differentially activated depending on the mutational status of the BRAF oncogene (Zheng et al., 2009), autophagy was a critical determinant of cell survival, making BRAF mutant cells especially sensitive to mitochondrial cell death initiated by Gamitrinib (Kang et al., 2007). This observation may have clinical relevance, as melanoma patients carrying a V600E BRAF mutation become invariably resistant to small-molecule BRAF inhibitors, pressing the need for alternative therapeutic targets to restore treatment responses in these settings.

ATP depletion results in insufficient energy available for protein posttranslational modifications (Kaufman et al., 2002), and in the case of mitochondrial proteotoxic stress, this triggered a canonical ER UPR (Hetz and Glimcher, 2009). This pathway was reproduced by pharmacologic uncoupling of mitochondrial membrane potential, in keeping with directional mitochondria-to-ER signaling, was partially reversed by high glucose, consistent with a causal role of defective ATP production in this process (Kaufman et al., 2002), and required LKB1-AMPK activation as part of bioenergetics signaling (Mihaylova and Shaw, 2011). The role of ER stress in cancer is complex, and prolonged activation of this pathway culminates with apoptosis contributed, at least in part, by transcriptional modulation of Bcl-2 proteins (Tabas and Ron, 2011). However, low-level, chronic ER stress may be beneficial for tumor growth (Ma and Hendershot, 2004), and the inducible ER chaperone GRP78 was identified here as an effector of tumor cell survival and proliferation during bioenergetics ER stress (Pfaffenbach and Lee, 2011). Cytoprotection by GRP78 may involve modulation of multiple antiapoptotic thresholds, including differential assembly of Bcl-2 homodimers (Zhou et al., 2011), and, as shown here, this pathway may become broadly exploited in genetically disparate cancers, correlating with shortened overall survival in patients with lung adenocarcinoma (this study), or prostate cancer (Tan et al., 2011). Regarding a potential role of other ER markers in disease outcome, high levels of eIF2α have been associated with improved survival in stage I, but not stages II–IV, NSCLC patients (He et al., 2011).

(I) LN229 cells were cultivated in the presence of the indicated increasing concentrations of glucose-containing medium without (None) or with Gamitrinib (5 μM) and analyzed by western blotting.
(J) LN229 cells were treated with the indicated concentrations of Gamitrinib in the presence (+) or absence (−) of sodium pyruvate (Pyr, 1 mM), and analyzed after 7 hr by western blotting.
See also Figure S4.

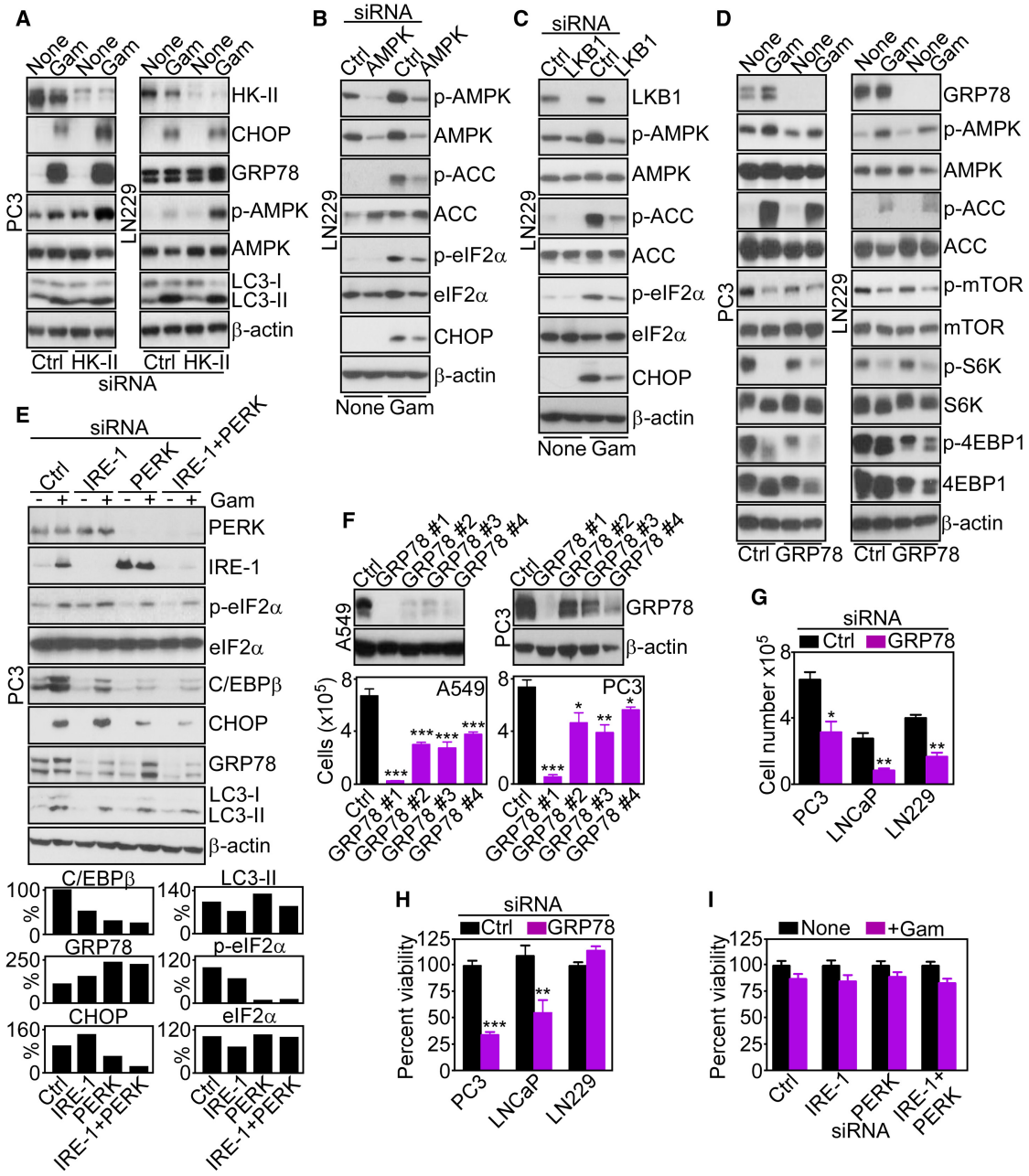

Figure 6. Functional Requirements of ER UPR Induced by Mitochondrial Proteotoxic Stress

(A–E) The indicated tumor cell lines were transfected with control siRNA (Ctrl), or with siRNA directed to HK-II (A), AMPK (B), LKB1 (C), GRP78 (D), or the ER stress sensors IRE-1 or PERK, alone or in combination (E), incubated in the presence or absence (None) of Gamitrinib (5 μM), and analyzed 24–48 hr after siRNA transfection by western blotting. The bar graphs in (E) show densitometric quantification of normalized C/EBPβ, CHOP, GRP78, LC3-II, or phosphorylated eIF2α bands in the presence of Gamitrinib. Basal eIF2α levels in the absence of Gamitrinib were also calculated.

(F) A549 or PC3 cells were transfected with control siRNA (Ctrl) or the indicated individual siRNA sequences to GRP78, and analyzed after 48 hr by western blotting. Bottom, siRNA-transfected cells as in the top images were analyzed for cell proliferation by direct cell counting. Mean ± SEM of three independent experiments. *$p < 0.05$; **$p < 0.01$; ***$p < 0.001$.

(G and H) The indicated tumor cell types were transfected with control siRNA (Ctrl) or GRP78-directed siRNA and analyzed for cell proliferation by direct cell counting (G) or cell viability by MTT (H). Mean ± SEM (n = 8 in [G] and 3 in [H]); *$p = 0.016$; **$p = 0.017–0.0055$; ***$p < 0.0001$.

(I) siRNA-transfected PC3 cells as in (E) were treated in the absence (None) or presence of 5 μM Gamitrinib and analyzed for cell viability by MTT. Mean ± SEM of replicates of a representative experiment from two independent determinations.

See also Figure S5.

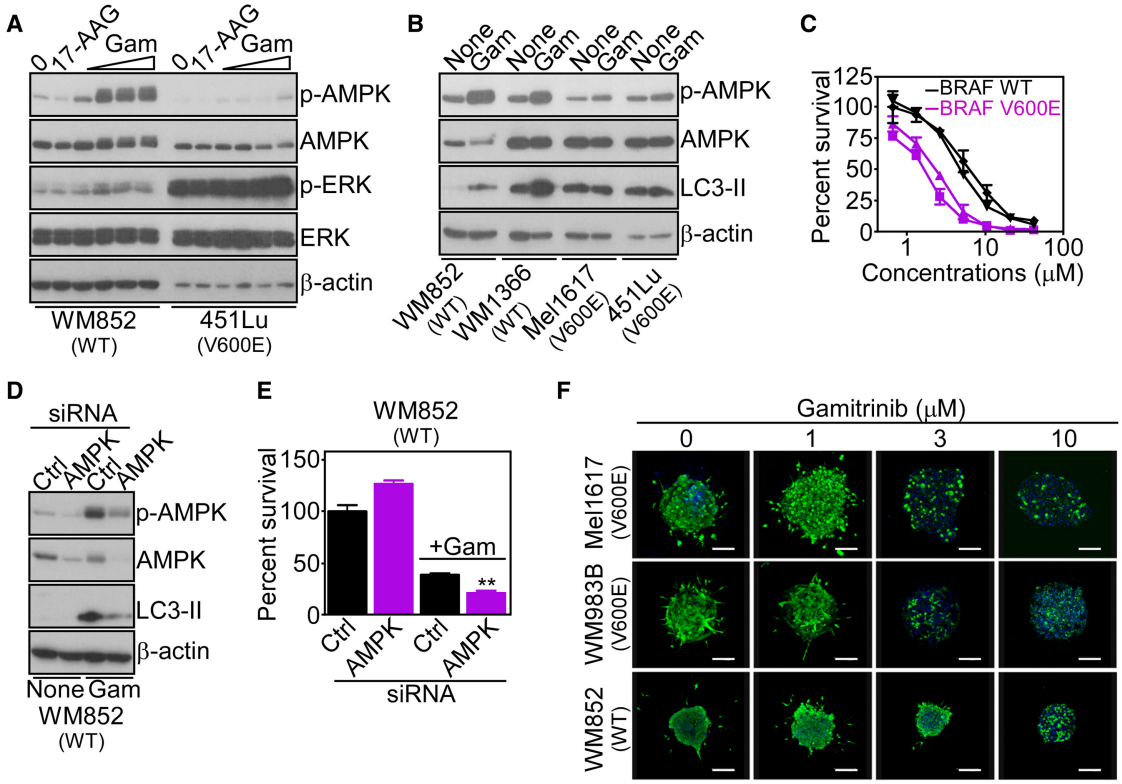

Figure 7. Regulation of Tumor Cell Survival by Mitochondrial Proteotoxic Stress

(A) WT or V600E mutant BRAF melanoma cell lines were treated with 17-AAG (10 μM) or Gamitrinib (1, 2.5, 5, or 10 μM) and analyzed after 5 hr by western blotting.

(B) The indicated melanoma cell types were incubated with Gamitrinib (5 μM) and analyzed after 9 hr by western blotting. None, untreated.

(C) WT (WM852, WM1366) or mutant BRAF (Me1617, 451Lu) melanoma cells were treated with Gamitrinib and analyzed after 16 hr for cell viability by MTT. Mean ± SD (n = 2).

(D) WM852 BRAF WT melanoma cells were transfected with control (Ctrl) or AMPK-directed siRNA, treated with Gamitrinib (5 μM), and analyzed by western blotting.

(E) WM852 melanoma cells transfected as in (D) were analyzed by MTT for Gamitrinib (10 μM)-mediated cell killing. Mean ± SEM (n = 3); **p = 0.002.

(F) Melanoma cells with the indicated BRAF genotype were grown as organotypic spheroids in 3D collagen-embedded matrices, incubated with the indicated concentrations of Gamitrinib, stained after 72 hr with calcein-AM (live cells; green) and Topro-3 (dead cells; blue), and analyzed by confocal laser scanning microscopy. Representative images were collected from one of two independent determinations.

See also Figure S6.

Together, the results presented here add complexity to HSP90 homeostasis (Taipale et al., 2010), uncovering a role of the mitochondrial pool(s) of these chaperones (Kang et al., 2007) in selective bioenergetics (Vander Heiden et al., 2009) and stress-response signaling (Hetz and Glimcher, 2009; Yang et al., 2011) in tumors. Although these mechanisms are critical for tumor growth, the pathophysiological context in which mitochondrial proteostasis (Siegelin et al., 2011) connects to bioenergetics and compensatory stress response in vivo remains to be fully elucidated. It may be speculated that the microenvironment of tumor growth, typically deprived of oxygen and nutrients, may produce a chronic degree of mitochondrial proteotoxic stress (Siegelin et al., 2011) that is further exacerbated by the higher biosynthetic needs of transformed cells and the unique structural environment of mitochondria (Haynes and Ron, 2010). In this context, the selective recruitment of HSP90s to tumor mitochondria (Kang et al., 2007) appears ideally poised to buffer organelle proteotoxic stress in general, and specifically to control the (re)folding of CypD (Green and Kroemer, 2004). In turn, this prevents permeability pore opening, especially against oxidative stimuli (Baines et al., 2005; Nakagawa et al., 2005), maintains ATP production via HK-II tethering (Vander Heiden et al., 2009), and connects to downstream survival mechanisms of autophagy (Yang et al., 2011) and GRP78 cytoprotection (Hetz and Glimcher, 2009; Yang et al., 2011). While this adaptive network promotes tumor maintenance in vivo, it may also offer tangible therapeutic prospects, as subcellular targeting of mitochondrial HSP90s is feasible and may selectively affect tumor cells, but not normal tissues (Kang et al., 2009).

EXPERIMENTAL PROCEDURES

Mitochondrial Protein Folding

Mitochondrial protein folding assays were performed as described (Moisoi et al., 2009). Briefly, mitochondrial fractions were isolated from vehicle or Gamitrinib-treated LN229 cells (5 μM for 12 hr) and suspended in equal volume of mitochondrial fractionation buffer containing increasing concentrations of CHAPS (0, 0.05, 0.1, 0.2, 0.5, 1, or 2%). Samples were incubated for 20 min on ice, and detergent-insoluble protein aggregates were

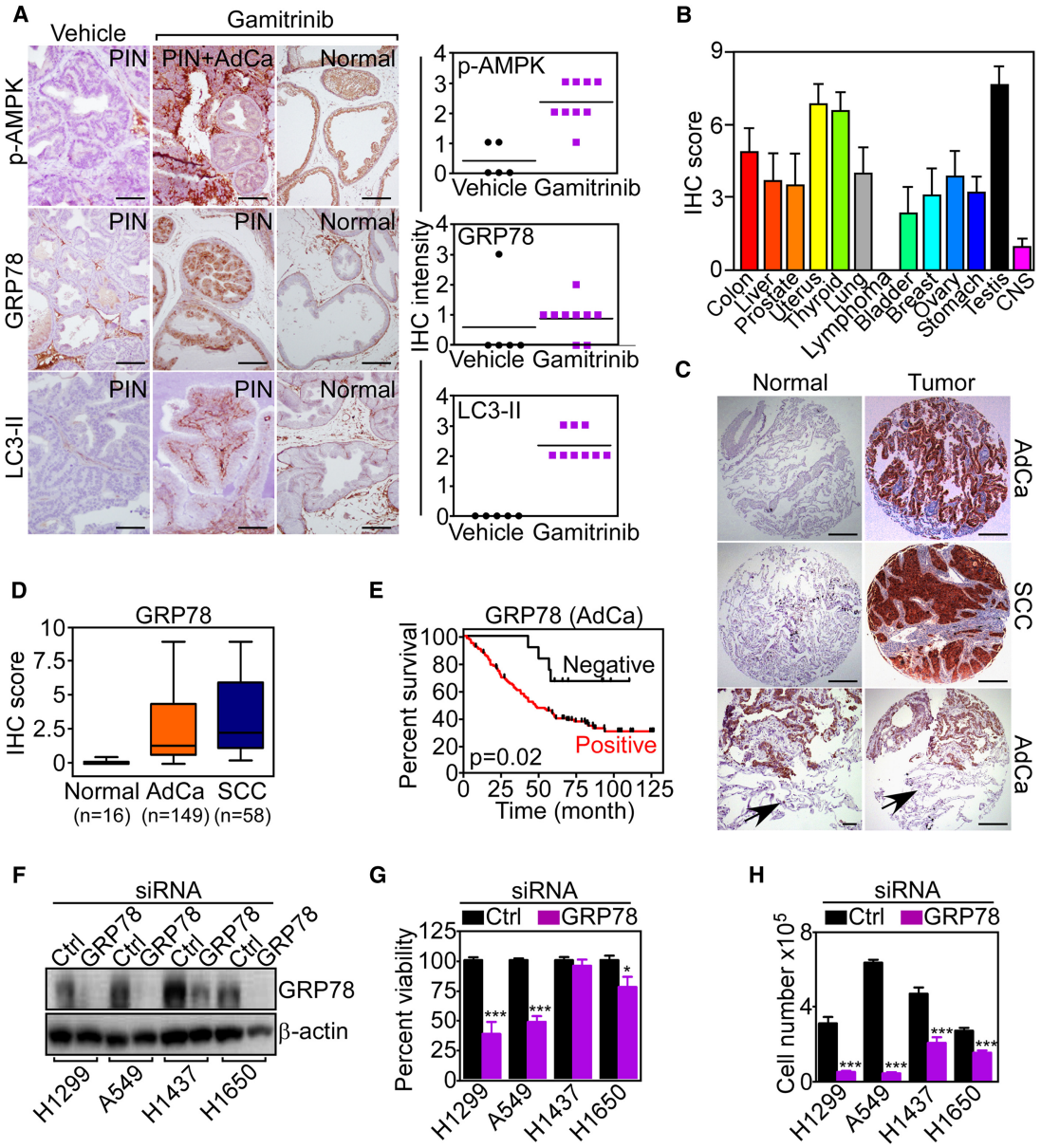

Figure 8. Activation of Mitochondrial Bioenergetics Signaling during Tumor Progression In Vivo

(A) Prostate samples from TRAMP mice treated systemically with vehicle or Gamitrinib were analyzed by immunohistochemistry with antibodies to phosphorylated AMPK (p-AMPK), GRP78, or LC3-II. The histological diagnosis of each prostate tissue section is indicated. Right: quantification of staining intensity for each condition. Scale bars, 50 μm.

(B) Expression of GRP78 in a universal tumor microarray was quantified by an immunohistochemistry (IHC) score. Each bar quantifies expression in the indicated tumor sites. CNS, central nervous system. Mean ± SEM of IHC score in each individual TMA core (n = 7).

(C) Immunohistochemical reactivity of GRP78 expression in a representative NSCLC-TMA. The bottom images show areas of normal lung parenchyma negative for GRP78 expression (arrows) adjacent to GRP78-positive lung cancer. Scale bars, 50 μm and 10 μm (bottom left).

(D) Summary of GRP78 expression in NSCLC or normal lung examined in this study. The number of cases for each histologic condition is indicated. In this series, 13 cases (6%) were not evaluable and 17 cases (8%) were negative for GRP78 expression. Bars correspond to median expression values of IHC scores with interquartile range. AdCa, adenocarcinoma; SCC, squamous cell carcinoma; IHC, immunohistochemistry. The statistical analysis for GRP78 expression in the various cohorts (t test) is as follows: NSCLC versus normal, $p = 1.37 \times 10^{-32}$; AdCa versus normal, $p = 1.49 \times 10^{-21}$; SCC versus normal, $p = 3.9 \times 10^{-13}$; AdCa versus SCC, p = 0.051.

(E) Patients with diagnosis of lung adenocarcinoma (AdCa) with no expression (negative) or high expression (positive) of GRP78 were analyzed for overall survival by the Kaplan-Meier method.

(F) The indicated lung adenocarcinoma cell types were transfected with control (Ctrl) or GRP78-directed siRNA and analyzed by western blotting.

(G and H) The indicated lung cancer cell lines were transfected as in (F) and analyzed for cell viability by MTT (G) or cell proliferation by direct cell counting (H). Mean ± SEM (n = 6). *p = 0.035; ***p = 0.0001–0.0002.

See also Figure S7 and Table S1.

isolated by centrifugation (20,000 × *g*) for 20 min and processed for further analysis.

Glucose and Lactate Determination

Glucose concentrations in cell culture media were determined using a glucose kit (Sigma-Aldrich). Briefly, 2×10^6 cells were seeded in 10 cm tissue-culture dishes for 48 hr and mixed with DMEM in the presence of Gamitrinib or 17-AAG (0–20 μM) for 4 hr; 200 μl aliquots of culture medium were then incubated with 1 ml assay mixture containing 1.5 mM NAD, 1 mM ATP, 1 U/ml HK, and 1 U/ml glucose-6-phosphate dehydrogenase (G6PDH). The glucose concentration was determined by measuring the amount of NAD reduced to NADH by G6PDH, and quantified spectrophotometrically at 340 nm wavelength. Extracellular lactate was measured by a colorimetric assay kit (Abcam). For these experiments, culture medium was replaced with DMEM containing vehicle (DMSO) or Gamitrinib (5 μM) for 5 hr. Changes in lactate concentrations were measured by analysis of lactate-dependent conversion of NADP to NADPH in the presence of excess lactate dehydrogenase (LDH) and were quantified by absorbance at 450 nm. All assays were performed at 25°C under conditions of linear lactate-limited NADPH formation.

Oxygen Consumption

Treated tumor cells were analyzed using a fluorescence oxygen-sensitive-probe-based oxygen measuring kit (Luxcel Bioscience). For these experiments, LN229 cells were plated at increasing cell density ($10–60 \times 10^4$/ml) on black-body, clear-bottom 96-well plates. The culture medium was replaced with 150 μl of phenol-free DMEM containing 10% fetal bovine serum in the presence of 17-AAG or Gamitrinib (10 μM). Cells were further incubated with an oxygen-sensing probe (10 pmol/well), and 100 μl of heavy mineral oil was added to each well to seal the samples from ambient oxygen. After 2 hr incubation at 37°C, oxygen consumption was determined by quantifying the probe fluorescence signal in each well using a plate reader (Beckman Coulter) with excitation and emission wavelengths at 370 nm and 625 nm, respectively.

ATP Measurement

Intracellular ATP concentrations were determined by a luciferin–luciferase method (Biochain) in a microplate luminometer (Beckman Coulter) against standard ATP solutions used as reference. In some experiments, PC3 or LN229 cells were incubated with sodium pyruvate (1 mM) for 7 hr in the presence of vehicle or Gamitrinib before determination of ATP production.

HK Activity

HK activity was measured as the total glucose-phosphorylating activity using a standard G6PDH-coupled assay kit (BioVision). Briefly, mitochondria isolated from Gamitrinib- or 17-AAG-treated LN229 cells, or cultures transfected with various siRNAs, were homogenized in cold PBS and then centrifuged at 1000 × *g* for 10 min at 4°C. HK activity was determined by analysis of G6PDH-dependent conversion of NADP to NADPH in the presence of excess G6PDH and 2 mM glucose, followed by quantification of absorbance at 450 nm. All assays were performed at 25°C under conditions of linear HK-limited NADPH formation.

Genetic Model of Prostate Cancer

All experiments involving vertebrate animals were approved by an Institutional Animal Care and Use Committee at the University of Massachusetts Medical School and The Wistar Institute. Activation of mitochondrial HSP90 signaling was investigated in immunocompetent TRAMP mice, as described (Kang et al., 2011).

Patient Samples

A series of 217 consecutive patients surgically treated for non-small-cell lung cancer (NSCLC) at Fondazione IRCCS Cà Granda Hospital (Milan, Italy) between 2000 and 2004 was available for this study. Informed consent was obtained from all patients enrolled, and the study was approved by an Institutional Review Board of the Fondazione IRCCS Cà Granda, Milan, Italy. Representative tissue blocks from consenting patients with various cancer diagnoses were used under IRB approval to construct the cancer universal TMA (CaU-TMA) and NSCLC TMAs. For the NSCLC-TMAs, four cores of each patient were included in the blocks, along with 16 cores of nonneoplastic lung parenchyma.

Statistical Analysis

Data were analyzed by means of two-sided unpaired t tests using a GraphPad software package (Prism 4.0) for Windows. For analysis of patient samples, groups were compared using the Wilcoxon signed-rank or Student's t test as univariate statistics. For overall survival analysis, the Kaplan-Meyer method was used. Patients negative for GRP78 (immunoreactivity score <0.25) were plotted separately from GRP78-positive cases (score ≥0.25), and the two-sided log-rank test was used to compare the two curves. Data are expressed as the mean ± SD or mean ± SEM of multiple independent experiments. A p value of ≤0.05 was considered statistically significant.

SUPPLEMENTAL INFORMATION

Supplemental Information includes seven figures, one table, and Supplemental Experimental Procedures and can be found with this article online at http://dx.doi.org/10.1016/j.ccr.2012.07.015.

ACKNOWLEDGMENTS

We thank Drs. Winklhofer and Fafournoux for providing luciferase reporter constructs and James Hayden for assistance with confocal microscopy. This work was supported by National Institutes of Health (NIH) Grants CA140043, CA78810, HL54131, and CA118005 (to D.C.A.) and Fondazione Cariplo (to S.B.). Support for Core Facilities utilized in this study was provided by Cancer Center Support Grant (CCSG) CA010815 to The Wistar Institute.

Y.C.C., M.C.C., S.L., J.C.G., T.D., and J.V. designed and carried out experiments. N.N.D. provided CypD knockout MEFs. L.S. provided clinical follow-up data. V.V., S.F., and S.B. provided pathological evaluation of the patient series and analysis of patient data. Y.C.C., M.C.C., S.L., N.D.D., J.V., M.H., L.R.L., S.B., and D.C.A. analyzed results. Y.C.C., M.C.C., S.L., and D.C.A. wrote the manuscript.

Received: October 21, 2011
Revised: April 23, 2012
Accepted: July 24, 2012
Published: September 10, 2012

REFERENCES

Baines, C.P., Kaiser, R.A., Purcell, N.H., Blair, N.S., Osinska, H., Hambleton, M.A., Brunskill, E.W., Sayen, M.R., Gottlieb, R.A., Dorn, G.W., et al. (2005). Loss of cyclophilin D reveals a critical role for mitochondrial permeability transition in cell death. Nature *434*, 658–662.

Egan, D.F., Shackelford, D.B., Mihaylova, M.M., Gelino, S., Kohnz, R.A., Mair, W., Vasquez, D.S., Joshi, A., Gwinn, D.M., Taylor, R., et al. (2011). Phosphorylation of ULK1 (hATG1) by AMP-activated protein kinase connects energy sensing to mitophagy. Science *331*, 456–461.

Gandhi, S., Wood-Kaczmar, A., Yao, Z., Plun-Favreau, H., Deas, E., Klupsch, K., Downward, J., Latchman, D.S., Tabrizi, S.J., Wood, N.W., et al. (2009). PINK1-associated Parkinson's disease is caused by neuronal vulnerability to calcium-induced cell death. Mol. Cell *33*, 627–638.

Green, D.R., and Kroemer, G. (2004). The pathophysiology of mitochondrial cell death. Science *305*, 626–629.

Gwinn, D.M., Shackelford, D.B., Egan, D.F., Mihaylova, M.M., Mery, A., Vasquez, D.S., Turk, B.E., and Shaw, R.J. (2008). AMPK phosphorylation of raptor mediates a metabolic checkpoint. Mol. Cell *30*, 214–226.

Haynes, C.M., and Ron, D. (2010). The mitochondrial UPR—protecting organelle protein homeostasis. J. Cell Sci. *123*, 3849–3855.

He, Y., Correa, A.M., Raso, M.G., Hofstetter, W.L., Fang, B., Behrens, C., Roth, J.A., Zhou, Y., Yu, L., Wistuba, I.I., et al. (2011). The role of PKR/eIF2α signaling pathway in prognosis of non-small cell lung cancer. PLoS ONE *6*, e24855.

Hetz, C., and Glimcher, L.H. (2009). Fine-tuning of the unfolded protein response: assembling the IRE1α interactome. Mol. Cell *35*, 551–561.

Hezel, A.F., and Bardeesy, N. (2008). LKB1; linking cell structure and tumor suppression. Oncogene *27*, 6908–6919.

Inoki, K., Zhu, T., and Guan, K.L. (2003). TSC2 mediates cellular energy response to control cell growth and survival. Cell *115*, 577–590.

Kang, B.H., Plescia, J., Dohi, T., Rosa, J., Doxsey, S.J., and Altieri, D.C. (2007). Regulation of tumor cell mitochondrial homeostasis by an organelle-specific Hsp90 chaperone network. Cell *131*, 257–270.

Kang, B.H., Plescia, J., Song, H.Y., Meli, M., Colombo, G., Beebe, K., Scroggins, B., Neckers, L., and Altieri, D.C. (2009). Combinatorial drug design targeting multiple cancer signaling networks controlled by mitochondrial Hsp90. J. Clin. Invest. *119*, 454–464.

Kang, B.H., Tavecchio, M., Goel, H.L., Hsieh, C.C., Garlick, D.S., Raskett, C.M., Lian, J.B., Stein, G.S., Languino, L.R., and Altieri, D.C. (2011). Targeted inhibition of mitochondrial Hsp90 suppresses localised and metastatic prostate cancer growth in a genetic mouse model of disease. Br. J. Cancer *104*, 629–634.

Kaufman, R.J., Scheuner, D., Schröder, M., Shen, X., Lee, K., Liu, C.Y., and Arnold, S.M. (2002). The unfolded protein response in nutrient sensing and differentiation. Nat. Rev. Mol. Cell Biol. *3*, 411–421.

Kurtoglu, M., Gao, N., Shang, J., Maher, J.C., Lehrman, M.A., Wangpaichitr, M., Savaraj, N., Lane, A.N., and Lampidis, T.J. (2007). Under normoxia, 2-deoxy-D-glucose elicits cell death in select tumor types not by inhibition of glycolysis but by interfering with N-linked glycosylation. Mol. Cancer Ther. *6*, 3049–3058.

Laderoute, K.R., Amin, K., Calaoagan, J.M., Knapp, M., Le, T., Orduna, J., Foretz, M., and Viollet, B. (2006). 5′-AMP-activated protein kinase (AMPK) is induced by low-oxygen and glucose deprivation conditions found in solid-tumor microenvironments. Mol. Cell. Biol. *26*, 5336–5347.

Leskovar, A., Wegele, H., Werbeck, N.D., Buchner, J., and Reinstein, J. (2008). The ATPase cycle of the mitochondrial Hsp90 analog Trap1. J. Biol. Chem. *283*, 11677–11688.

Ma, Y., and Hendershot, L.M. (2004). The role of the unfolded protein response in tumour development: friend or foe? Nat. Rev. Cancer *4*, 966–977.

Machida, K., Ohta, Y., and Osada, H. (2006). Suppression of apoptosis by cyclophilin D via stabilization of hexokinase II mitochondrial binding in cancer cells. J. Biol. Chem. *281*, 14314–14320.

Majewski, N., Nogueira, V., Bhaskar, P., Coy, P.E., Skeen, J.E., Gottlob, K., Chandel, N.S., Thompson, C.B., Robey, R.B., and Hay, N. (2004). Hexokinase-mitochondria interaction mediated by Akt is required to inhibit apoptosis in the presence or absence of Bax and Bak. Mol. Cell *16*, 819–830.

Mayer, M.P. (2010). Gymnastics of molecular chaperones. Mol. Cell *39*, 321–331.

Mihaylova, M.M., and Shaw, R.J. (2011). The AMPK signalling pathway coordinates cell growth, autophagy and metabolism. Nat. Cell Biol. *13*, 1016–1023.

Moisoi, N., Klupsch, K., Fedele, V., East, P., Sharma, S., Renton, A., Plun-Favreau, H., Edwards, R.E., Teismann, P., Esposti, M.D., et al. (2009). Mitochondrial dysfunction triggered by loss of HtrA2 results in the activation of a brain-specific transcriptional stress response. Cell Death Differ. *16*, 449–464.

Nakagawa, T., Shimizu, S., Watanabe, T., Yamaguchi, O., Otsu, K., Yamagata, H., Inohara, H., Kubo, T., and Tsujimoto, Y. (2005). Cyclophilin D-dependent mitochondrial permeability transition regulates some necrotic but not apoptotic cell death. Nature *434*, 652–658.

Pfaffenbach, K.T., and Lee, A.S. (2011). The critical role of GRP78 in physiologic and pathologic stress. Curr. Opin. Cell Biol. *23*, 150–156.

Richter, K., Reinstein, J., and Buchner, J. (2007). A Grp on the Hsp90 mechanism. Mol. Cell *28*, 177–179.

Robey, R.B., and Hay, N. (2006). Mitochondrial hexokinases, novel mediators of the antiapoptotic effects of growth factors and Akt. Oncogene *25*, 4683–4696.

Rodina, A., Vilenchik, M., Moulick, K., Aguirre, J., Kim, J., Chiang, A., Litz, J., Clement, C.C., Kang, Y., She, Y., et al. (2007). Selective compounds define Hsp90 as a major inhibitor of apoptosis in small-cell lung cancer. Nat. Chem. Biol. *3*, 498–507.

Siegelin, M.D., Dohi, T., Raskett, C.M., Orlowski, G.M., Powers, C.M., Gilbert, C.A., Ross, A.H., Plescia, J., and Altieri, D.C. (2011). Exploiting the mitochondrial unfolded protein response for cancer therapy in mice and human cells. J. Clin. Invest. *121*, 1349–1360.

Tabas, I., and Ron, D. (2011). Integrating the mechanisms of apoptosis induced by endoplasmic reticulum stress. Nat. Cell Biol. *13*, 184–190.

Taipale, M., Jarosz, D.F., and Lindquist, S. (2010). HSP90 at the hub of protein homeostasis: emerging mechanistic insights. Nat. Rev. Mol. Cell Biol. *11*, 515–528.

Tan, S.S., Ahmad, I., Bennett, H.L., Singh, L., Nixon, C., Seywright, M., Barnetson, R.J., Edwards, J., and Leung, H.Y. (2011). GRP78 up-regulation is associated with androgen receptor status, Hsp70-Hsp90 client proteins and castrate-resistant prostate cancer. J. Pathol. *223*, 81–87.

Trepel, J., Mollapour, M., Giaccone, G., and Neckers, L. (2010). Targeting the dynamic HSP90 complex in cancer. Nat. Rev. Cancer *10*, 537–549.

Vander Heiden, M.G., Cantley, L.C., and Thompson, C.B. (2009). Understanding the Warburg effect: the metabolic requirements of cell proliferation. Science *324*, 1029–1033.

Villanueva, J., Vultur, A., Lee, J.T., Somasundaram, R., Fukunaga-Kalabis, M., Cipolla, A.K., Wubbenhorst, B., Xu, X., Gimotty, P.A., Kee, D., et al. (2010). Acquired resistance to BRAF inhibitors mediated by a RAF kinase switch in melanoma can be overcome by cotargeting MEK and IGF-1R/PI3K. Cancer Cell *18*, 683–695.

Wolf, A., Agnihotri, S., Micallef, J., Mukherjee, J., Sabha, N., Cairns, R., Hawkins, C., and Guha, A. (2011). Hexokinase 2 is a key mediator of aerobic glycolysis and promotes tumor growth in human glioblastoma multiforme. J. Exp. Med. *208*, 313–326.

Wullschleger, S., Loewith, R., and Hall, M.N. (2006). TOR signaling in growth and metabolism. Cell *124*, 471–484.

Yang, S., Wang, X., Contino, G., Liesa, M., Sahin, E., Ying, H., Bause, A., Li, Y., Stommel, J.M., Dell'antonio, G., et al. (2011). Pancreatic cancers require autophagy for tumor growth. Genes Dev. *25*, 717–729.

Zheng, B., Jeong, J.H., Asara, J.M., Yuan, Y.Y., Granter, S.R., Chin, L., and Cantley, L.C. (2009). Oncogenic B-RAF negatively regulates the tumor suppressor LKB1 to promote melanoma cell proliferation. Mol. Cell *33*, 237–247.

Zhou, H., Zhang, Y., Fu, Y., Chan, L., and Lee, A.S. (2011). Novel mechanism of anti-apoptotic function of 78-kDa glucose-regulated protein (GRP78): endocrine resistance factor in breast cancer, through release of B-cell lymphoma 2 (BCL-2) from BCL-2-interacting killer (BIK). J. Biol. Chem. *286*, 25687–25696.